Chem

CellPress

Article

Producing oxygen and fertilizer with the Martian atmosphere by using microwave plasma

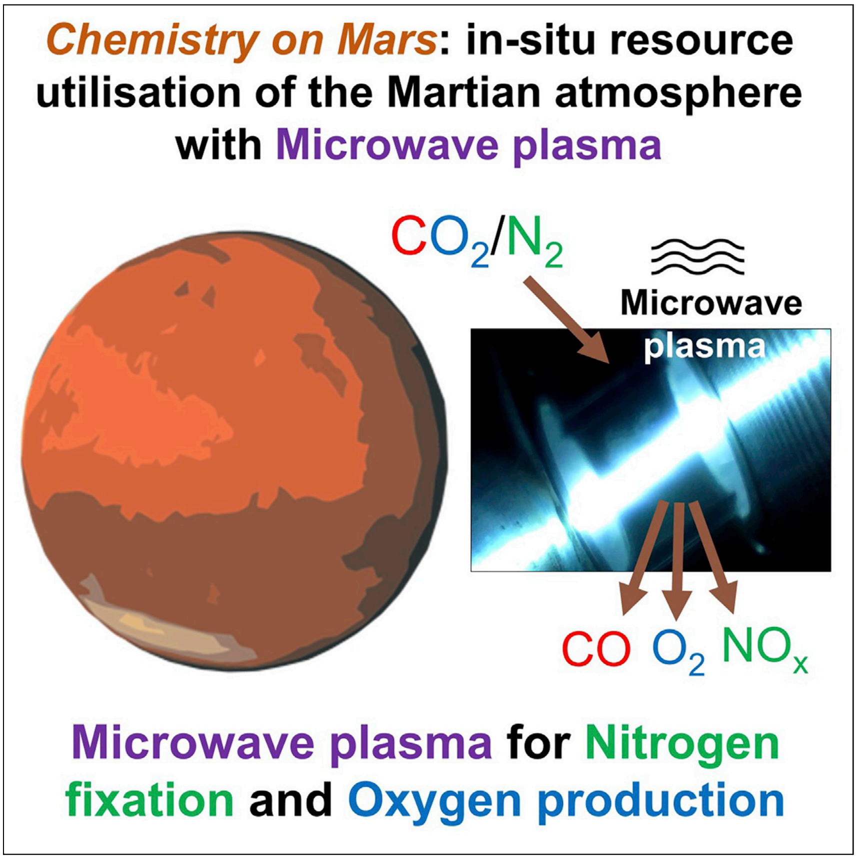

Kelly et al. explore the potential of microwave-plasma-based *in situ* resource utilization (ISRU) of the Martian atmosphere with a focus on the novel possibility of fixing nitrogen (i.e., fertilizer production). Oxygen liberated through carbon dioxide dissociation facilitates the fixation of the nitrogen fraction. This demonstrates a novel process for sourcing a key macronutrient for future agriculture. Furthermore, oxygen production rates for a microwave plasma are found to be very promising in comparison with those of the Mars Oxygen *In Situ* Resource Utilization Experiment (MOXIE).

9 INDUSTRY, INNOVATION AND INFRASTRUCTURE

Seán Kelly, Claudia Verheyen, Aidan Cowley, Annemie Bogaerts

sean.kelly@uantwerpen.be

Highlights

The novel possibility of fixing nitrogen on Mars by using plasma is explored

Nitrogen fixation is facilitated by oxygen liberated through CO_2 dissociation

Oxygen production rates for microwave plasma are very promising in comparison with MOXIE

Kelly et al., Chem *8*, 2797–2816
October 13, 2022 © 2022 Elsevier Inc.
https://doi.org/10.1016/j.chempr.2022.07.015

Chem

CellPress

Article

Producing oxygen and fertilizer with the Martian atmosphere by using microwave plasma

Seán Kelly,[1,4,*] Claudia Verheyen,[1,2] Aidan Cowley,[3] and Annemie Bogaerts[1]

SUMMARY

We explore the potential of microwave (MW)-plasma-based *in situ* utilization of the Martian atmosphere with a focus on the novel possibility of fixing N_2 for fertilizer production. Conversion in a simulant plasma (i.e., ~96% CO_2, ~2% N_2, and ~2% Ar), performed under energy conditions similar to those of the Mars Oxygen *In Situ* Resource Utilization Experiment (MOXIE), currently on board NASA's Perseverance rover, demonstrates that O/O_2 formed through CO_2 dissociation facilitates the fixation of the N_2 fraction via oxidation to NO_x. Promising production rates for O_2, CO, and NO_x of 47.0, 76.1, and 1.25 g/h, respectively, are recorded with corresponding energy costs of 0.021, 0.013, and 0.79 kWh/g, respectively. Notably, O_2 production rates are ~30 times higher than those demonstrated by MOXIE, while the NO_x production rate represents an ~7% fixation of the N_2 fraction present in the Martian atmosphere. MW-plasma-based conversion therefore shows great potential as an *in situ* resource utilization (ISRU) technology on Mars in that it simultaneously fixes N_2 and produces O_2.

INTRODUCTION

The expansion of *in situ* resource utilization (ISRU) technology[1–8] will be a key enabler for both private- and public-funded space exploration of planets such as Mars. The prohibitive cost of bringing fuel, O_2, and food to Mars greatly motivates exploitation of local resources. The European Space Agency's (ESA's) Ariane 5G heavy lift rocket, for instance, has a payload cost of ~$10,000/kg to reach low Earth orbit (LEO).[9] The additional costs of sending each kilogram from LEO to Mars is estimated at over ten times the initial LEO costs,[10] leading to a conservative estimate of $100,000/kg. This is further compounded by the ~26 month launch window between Earth and Mars (i.e., the Hohmann transfer orbit), requiring significantly more resources for both human and two-way robotic missions to the red planet than what was needed during the Apollo Lunar missions (which took just over 8 days from lift off to splash down). Such staggering costs emphasize the need to gain resources *in situ* by bringing the means of production rather than traditional supply-dominated payloads. Leveraging technologies for ISRU by "living off the land" is therefore a central tenet for future space enterprises in the hope of efficiently utilizing locally available renewable electricity, such as solar power, to harvest and process native resources. The ISRU paradigm therefore opens many new possibilities for future space exploration.[11,12]

In 2021, the National Aeronautics and Space Administration's (NASA's) Martian rover Perseverance performed the Mars Oxygen *In Situ* Resource Utilization

THE BIGGER PICTURE

The concept of "living off the land" is key for future space enterprises to planets such as Mars. The prohibitive cost of bringing fuel, oxygen, and food greatly motivates exploitation of resources locally, where chemistry must be performed *in situ*. In this work, we explore the potential of MW-plasma-based ISRU of the Martian atmosphere with a focus on the novel possibility of fixing nitrogen (i.e., fertilizer production). Conversion in a plasma ignited with a Martian atmosphere mix (consisting mostly of carbon dioxide with 2% nitrogen) is performed under energy conditions similar to those of MOXIE, currently on board NASA's Perseverance rover. We find that oxygen liberated through carbon dioxide dissociation facilitates the fixation of the nitrogen fraction. This demonstrates a novel process for sourcing a key macronutrient for agriculture. Furthermore, oxygen production rates are found to be very promising in comparison with those of MOXIE.

Experiment (MOXIE),[13] producing for the first time extra-terrestrial O_2 by using solar-harvested electricity. This milestone event is set to expand innovation in technologies to harvest Martian resources for fuel, life support, and materials over the coming decades. The solid oxide electrolysis cell (SOEC) component of MOXIE demonstrated the production of ~6 g of O_2 from compressed Martian ambient[14,15] by using a full sol energy allocation of 1 kWh (further details are given in Figure S1). Human consumption of O_2 is about 1 kg/day,[16,17] whereas utilization of O_2 in a fuel mixture (e.g., Methalox) to power a Mars ascent vehicle (MAV) could require thousands of tons of fuel.[14,18,19] Clearly, achieving the aspirations of future ISRU-based missions will require significant scale-up. MOXIE is based on SOEC technology, and because of the long start-up requirements (~2 h), the technique is largely inflexible to fluctuating energy production and so requires battery storage from any local renewable energy harvested on Mars. Techniques such as plasma-based gas conversion,[20,21] which can match production with the availability of renewable electricity (i.e., fast start-up time), therefore hold great potential for ISRU applications on the red planet.

Compared with Earth-bound climes, Mars, whose atmosphere is ~96% CO_2, ~2% N_2, and ~2% Ar,[22,23] provides quite favorable low-pressure (~1% of Earth's atmosphere) and -temperature (~0°C to <-60°C) conditions[22,23] for efficient plasma conversion. To date, however, the potential for this enticing technology has remained largely unexplored in an ISRU context.[24–31] Plasma-based O_2 generation and membrane extraction have previously been proposed with direct current (DC) plasma by Wu et al.[24] Gruenwald[25,26] envisaged the use of plasma technology by early Martian settlers for a wide range of applications, including O_2 production. More recent reports by Guerra et al.[27,28] have again demonstrated the potential of DC plasmas under Martian conditions, reiterating the benefits of using the ambient conditions for O_2 production. Premathilake et al. reported on the use of a DC plasma generated *in situ* of a thin silver membrane, which enabled partial oxygen removal.[29] Moses et al.[30] uniquely suggested the harvesting of plasma-produced O_2 during the landing descendant to Mars, where solid oxide cell technology could be incorporated into the heat shield to capture O_2. The potential use of microwave (MW) plasma under Martian conditions was recently explored in the Plasma Extraction of O_2 from Mars Atmosphere (PEOMA) project by Wheeler et al., supported by NASA.[31] Their experimental study, which focused on O_2 production, showed the feasibility of high levels of CO_2 conversion under low Martian pressure (i.e., with a low gas-flow rate). The energy efficiencies reported via conference proceedings[31] were, however, quite low (i.e., <10%). This contradicts previous studies of CO_2 plasma conversion at low pressures (i.e., close or below Martian ambient conditions), which claimed both high efficiency and high conversion levels, even up to 90% at supersonic flow conditions, as reported in the 1980s,[32] although the latter findings have not been reproduced to date.[33–35] The proposal for N_2 fixation (NF) with the Martian atmosphere using plasma, to the best of our knowledge, has not been previously interrogated. This intriguing prospect will therefore be of particular focus in this work.

Artificial NF is a cornerstone of modern civilization and currently sustains over 40% of Earth's population.[36,37] Unlike the other key macronutrients for plant growth, such as K and P, which have been discovered by soil sampling,[38–43] N is a rate-limiting nutrient for plant growth and is notably absent from the Martian regolith. Recent botanical experiments using Martian regolith simulants[38,41] have highlighted that seed germination and plant growth could be possible in controlled environments, such as an underground greenhouse. Future utilization of Martian regolith as a

[1] Research group PLASMANT, Department of Chemistry, University of Antwerp, Universiteitsplein 1, 2610 Antwerp, Belgium

[2] Chimie des Interactions Plasma-Surface (ChIPS), CIRMAP, Université de Mons, 23 Place du Parc, 7000 Mons, Belgium

[3] European Astronaut Centre, European Space Agency, 51147 Linder Höhe, Germany

[4] Lead contact

*Correspondence: sean.kelly@uantwerpen.be

https://doi.org/10.1016/j.chempr.2022.07.015

farming substrate will therefore require production of N_2-based fertilizer as a key enabler for plant growth to sustain future habitats.[7,38,41,44] Another important potential use for NF on Mars is the production of explosives with potential use for excavations and active seismology studies.[45,46]

On Earth, industrial-scale NF is at present achieved via the Haber-Bosch (H-B) process (producing ammonia) in combination with the Ostwald process (converting ammonia to nitric acid).[47] This energy-intensive process, fueled by natural gas (i.e., methane), has dominated artificial fertilizer production for almost a century and has enabled crop yield enhancements, which currently nourish a large proportion of the world population.[48] Given the exceptional stability of the N_2 triple bond, the H-B process is an energy-intensive chemical process that accounts for ~2% of the world's energy consumption, consumes ~3% of the global natural-gas output, and as a result, emits more than 300 million tons of CO_2 annually.[48] Recently, efforts to find H-B alternatives that are not reliant on fossil fuels have expanded, including significant interest in plasma technology.[20,36,37,49]

The large-scale use of plasmas to fix N_2 on Earth for fertilizer production goes back to the Birkeland-Eyde (B-E) process of producing nitric acid and was first developed in the early 20th century.[50–52] The B-E process involved the conversion of air to NO_x in an electric arc formed inside an electromagnet followed by an oxidation stage where the remaining NO was converted to NO_2 in settling tanks (i.e., a relatively slow reaction preferable at reduced temperatures). This stage was followed by NO_2 hydrolysis in large water-absorption towers packed with quartz segments, eventually producing a solution of HNO_3. The industrialized B-E process produced ~2% NO_x with an energy consumption for the NO_x plasma synthesis stage of 2.4–3.1 MJ/mol. The absorption stages added approximately 30%–40% additional energy overhead.[47,48,51]

A revival of research interest in plasma-based NF (i.e., a 21st century B-E process) has occurred recently with the expanding availability of renewable electricity and intense efforts to mitigate anthropogenic climate change.[48,53] Recently,[36] we showed very promising metrics for plasma NO_x production and energy cost (under Earth conditions), reaching 3.8% total NO_x concentration at a production rate of 0.77 L/min for ~2 MJ/mol energy cost, by using atmospheric-pressure MW plasmas. To our knowledge, this is the lowest energy cost reported in the literature for atmospheric pressure plasmas at significant NO_x concentrations. Note that we incorporated modern advancements in MW technology by employing a solid-state amplifier to power the reactor. Of course, such contemporary technology (and indeed MW technology) was not available when the B-E process was developed in the early 20th century.[54] Further, solid-state technology can significantly reduce the size and mass associated with MW-powered plasma generation and is therefore much more suitable to meeting the constraints of space deployment.[55] Solid-state power supplies are not only more compact but, as a result of superior control (i.e., over frequency and power), also enable compact plasma reactors by reducing the need for "bulky" waveguide components (e.g., plasma lighting applications[56]). A magnetron-based plasma reactor with a volume of ~25 L and mass of, say, ~50 kg could be reduced to 5 L and 5 kg.[57]

MW-generated plasmas offer the desirable characteristics[58] of high ionization fraction (i.e., electron density) coupled with relatively low mean electron energies. The electric field generated by the applied MW power selectively heats the electrons because of their small mass. Furthermore, the electron energy of 1–3 eV, combined with high electron density, gives rise to efficient vibrational and electronic excitation, which can in turn significantly promote efficient (i.e., non-thermal) dissociation routes in gases such as N_2.[53] Along with CO_2 conversion to O_2 and CO, the potential of plasma-based NF by oxidation of the N_2 content (2%) available in the Martian ambient provides a potential avenue for NF, which has to date not been explored. Vibrational and electronic excitation of the N_2 fraction in the Martian atmosphere can lower the threshold for breaking the extremely stable N_2 triple bond (~9.8 eV), which can then be oxidized by O/O_2 formed upon conversion of the large amounts of CO_2 present in the Martian atmosphere.

Compared with low-frequency plasma reactor designs, MW plasma technology offers a very-high overall power transmission efficiency.[21] In low-frequency plasma reactors, much of the electrical power can be lost in resistors and reflections as a result of impedance mismatching (dissipating as heat or nuisance radiation). Even DC-powered plasmas typically have an alternating voltage and current response (due to the resistive capacitive [RC] characteristics of the dynamic plasma and its circuit interaction). Previous studies on plasma-based gas conversion only considered the absorbed plasma power[21] when calculating the energy cost of conversion, which disregards a very large fraction of the real power wasted through transmission to the plasma (e.g., losses can be >50% of the overall system power for poorly matched designs that use high-resistance components to ballast plasma instabilities), but for practical applications, the input power should be considered, thus accounting also for the transmission efficiency of the power supply. MW plasma using solid-state technology can now sustain transmission efficiencies of >70% with ten times longer lifetimes than magnetron technologies, which degrade in performance comparatively quickly over time. The electromagnetic shielding of high-frequency MW discharges is also much more straightforward than low-frequency plasma devices, which present a considerable challenge in terms of minimizing electromagnetic interference (EMI) to neighboring electronics (e.g., EMI from arc welders operating at DC and kHz AC is a common nuisance[59,60]). We therefore believe that MW plasma generated with state-of-the-art low-mass, small-footprint solid-state amplifiers is the “technology of choice” for future missions deploying plasma-based gas-conversion technologies to Mars and beyond.

In this work, we explore the feasibility of NF on Mars by *in situ* leveraging the indigenous atmosphere in combination with the co-conversion of CO_2 to CO and O_2 for generating resources for fertilizers, fuels, and life-support systems by means of experiments benchmarked against MOXIE operating conditions and supported by chemical kinetics modeling to reveal the underlying mechanism.

RESULTS AND DISCUSSION

The aim of this investigation is to highlight the potential of MW plasma technology for ISRU on Mars. In particular, besides CO_2 conversion into CO and O_2, we also show the novel possibility for NF, the most energy-intensive aspect of fertilizer production and therefore a key requirement for nourishing any potential future Martian settlers. In the first section, we present the results for our MW plasma experiments using a Martian atmosphere mixture; in the second section, we use our corresponding numerical modeling to reveal the underlying mechanisms. This is followed by a discussion outlining possible utilization scenarios for plasma-based ISRU on Mars. Finally, a conclusion is given.

MW-plasma-based conversion in a Martian atmosphere

The operating conditions for our MW plasma reactor are inspired by the current MOXIE on board NASA’s Perseverance rover.[14] MOXIE operates with an energy

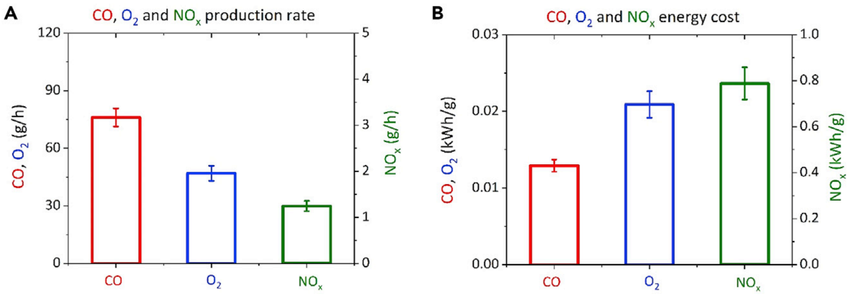

Figure 1. Absolute production rates and energy cost from the experiment

(A) Absolute production rates (g/h) of CO, O_2, and NO_x.

(B) Equivalent energy cost (kWh/g) in a MW plasma using a Martian simulant mixture of $CO_2/N_2/Ar$ (96/2/2%) at 10 L/min flow rate, 0.34 bar pressure, and 1 kW absorbed power.

Note that the NO_x data are indicated on the right-hand y axes.

allocation of 1 kWh by using a full sol worth of solar-harvested electricity. The solid oxide cell apparatus (known as SOEC), which performs the dissociation and purification, specifies an operating pressure ranging from 260 to 760 Torr (or 0.34–1 bar). The lower range of 0.34 bar is incorporated here for our plasma-operating conditions. In our setup, a vacuum system lowers the pressure inside the reactor to ~0.34 bar while using a typical swirling mass flow rate of 10 L/min to operate the reactor.[36] MOXIE uses lower mass flow rates given the operation conditions of the Martian atmosphere, where gases are compressed from the ambient conditions (~0.01 bar) to a higher pressure (i.e., 0.34–1 bar) inside the SOEC compartment. In spite of such differences, the key parameters of pressure and power are comparable in both cases, and thus our investigation serves to gain insight into possible conversion rates and energy costs by using plasma-based gas-conversion technology under rover energy conditions.

In Figure S1, we show graphical results of the historic MOXIE for O_2 production completed during April 2021.[15] MOXIE operating at a power of 300 W[14] over 3.3 h of operation (i.e., ~12,000 s) produced 5.4 g of O_2. This encompassed a 2 h warm-up period followed by ~1 h of O_2 generation. This yielded an O_2 production rate of ~1.6 g/h at an energy cost of 0.19 kWh/g. The overall O_2 produced (i.e., 5.4 g) during the test on April 20, 2021 (Sol 70 of the Martian year), used the 1 kWh energy allocation available to MOXIE from solar electricity harvested by panels on the Perseverance rover. Note that MOXIE operates at 300 W, whereas our MW plasma operated at 1 kW. However, we compare the two processes in terms of energy usage rather than power. Indeed, the MOXIE results from April 2021 (used here as a benchmark) consumed ~1 kWh of solar energy, which was applied at a rate of 300 W for ~12,000 s (~3.33 h). In comparison, our plasma operates at an energy deposition rate of 1 kW, which should run for 1 h to use the same 1 kWh energy as MOXIE. Since our comparison of production rates is made on the basis of the energy required per gram of CO, O_2, and NO_x produced (i.e., kWh/g), the disparate operating powers are not of particular concern.

In Figure 1A, we present the production rates of CO, O_2, and NO_x (i.e., sum of NO and NO_2) measured in the plasma exhaust for an inlet mass flow rate of 10 L/min (i.e., 1.131 kg/h CO_2, 30 g/h N_2, and 21.4 g/h Ar mass flow rate for a Martian mixture in a ratio of 96%/2%/2%) at (absorbed) plasma power of 1 kW. We measured production rates of 47.0 $\pm$ 3.9 g/h for O_2 and 76.1 $\pm$ 4.7 g/h for CO. The conversion of CO_2 was measured to be 9.4% $\pm$ 0.4%, and corresponding yields for O_2 and CO were measured as 5.2% ± 0.2% and 9.7% ± 0.6%, respectively; hence, the latter is approximately two times the O_2 value, which is in line with the stoichiometry of CO_2 splitting. Notably, the production rates, conversion, and product yields were adjusted for the gas expansion, which was measured as a ~5% increase of the inlet mass flow (i.e., $\alpha = 1.05$) (see Equation 4).

Figure 1B shows that the corresponding energy cost for the production of CO and O_2 is 0.0129 ± 0.0008 and 0.021 ± 0.002 kWh/g, respectively. Hence, the plasma produces O_2 at an energy cost about an order of magnitude smaller than in the recent MOXIE test, which reported 0.19 kWh/g (see Figure S1), and the O_2 production rate (47.0 g/h) is ~30 times higher than that in the MOXIE test (i.e., ~1.6 g/h). Plasma-based ISRU therefore shows much promise in comparison with SOEC production under comparable energy conditions. Note, however, that the energy gains demonstrated here do not account for the considerable cost of gas compression and separation or the energy losses of the solid-state MW power supply employed in this study, which has an efficiency of ~50%.[61] The energy cost of compressing the Martian atmosphere by MOXIE, carried out with a scroll pump, is approximately one-third of the total energy cost (i.e., ~0.06 kWh/g).[14] It is more difficult to estimate the energy cost of separation, but using the heat available in the plasma exhaust ($T_{exhaust} > 1,000$ K; see discussion below) will be key. Utilization of this energy could enable the use of O_2-separation technologies, which operate at high temperature. This includes emerging technologies such as oxygen transport membranes[62] or, indeed, more mature techniques such as SOECs. Hence, synergies with such O_2-separation technologies, enabling production of a pure O_2 stream, and plasma technology could yield very interesting pathways for future innovations. The findings presented here therefore strive to highlight and inspire further interrogation of this potential.

Figure 1A shows the total NO_x production rate as ~1.25 g/h and an equivalent concentration in the exhaust mixture of 1,320 ± 105 ppm (or 0.13%). NO and NO_2 are the primary species produced with a NO/NO_2 ratio of ~3.4. Notably, no other N_xO_y species (e.g., N_2O) were detected in measurable quantities. This produced NO_x concentration corresponds to ~7% of the N_2 inflow being fixed. The corresponding energy cost for NO_x production is ~0.79 kWh/g (see Figure 1B). This is considerably higher than the energy cost of O_2 production, which is expected given the low fraction of N_2 available in the Martian atmosphere, but at least it serves to give insight into what is possible with plasma-based NF on Mars using plasma technology. On Earth, the H-B process fixes about 171 teragrams (Tg) of N_2 per year, 70% of which is used for fertilizers (i.e., 84.7 Tg).[63] The utilization of this fixed N_2 (albeit very inefficiently[64,65]) supports at least ~2.8 billion people (i.e., ~40% of the current world population of 7.2 billion) for their food production. On this (Earth) basis, the estimated needs of a Martian settler are ~3 kg N/year or 8.2 g/day, and given an energy cost of 0.79 kWh/g for NO_x production shown in Figure 1, this amounts to ~6.5 kWh/day or ~2.36 MWh/year of energy expenditure. The cost of producing the ~1 kg of O_2 required daily per person[16] to sustain life on Mars can be similarly estimated as ~20 kWh/day or ~7.3 MWh/year with the energy cost of ~0.02 kWh/g for O_2, presented in Figure 1. The average daily energy needs for an Earth citizen today are about ~58 kWh,[66] where at least 1% of global energy is used for the production of nitrogen-based fertilizer (i.e., ~0.58 kWh).[67] Future Martian settlers will have much higher energy needs than their Earth neighbors. According to our estimates, as detailed above (i.e., ~6.5 kWh/day for NO_x [fertilizer] production and ~20 kWh/day for O_2 production [life support]), nitrogen fertilizers and O_2 alone

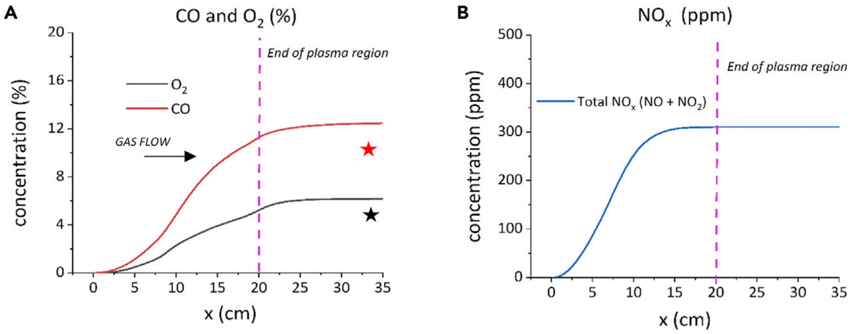

Figure 2. Calculated species levels from numerical modeling

Calculated CO, O_2 (A), and NO_x (B) product concentrations as a function of position in and after the MW plasma using a Martian simulant mixture of $CO_2/N_2/Ar$ (96%/2%/2% at a 10 L/min flow rate, 0.34 bar pressure, and 1 kW absorbed power). The measured CO and O_2 concentrations (downstream, hence after the plasma) are indicated with stars in (A) for comparison. The measured NO_x concentration is not added in (B) because there is still quite a large discrepancy with the calculated value (see text). Note: the direction of gas flow through the plasma is along the positive x direction.

will require ~27 kWh/day, i.e., almost half the total average that Earth residents use today (around 58 kWh; see above).

We measured the exhaust temperature from the plasma by using a k-type thermocouple positioned at ~10 cm outside the plasma and afterglow region (i.e., inside the gas connector shown in Figure 3B on the right side). We recorded a steady-state temperature of ~782°C (or ~1,055 K) for 1 kW absorbed MW power. Note that our gas analysis was performed after the plasma reactor was in operation for at least 15 min, after which time the exhausted gas temperature stabilized, indicating that the reactor reached a steady-state operation, although production rates of CO, O_2, and NO_x stabilized much faster (~10 s) than temperature. Utilization of this heat downstream presents an opportunity to reduce overall energy costs when this energy could be efficiently recovered,[68] for example, to heat the incoming gas before plasma conversion (with benefits to CO_2 and N_2 dissociation) or to provide heat energy for another chemical reaction or system downstream. In addition, we plan to explore synergies with O_2-separation technologies, which operate at high temperatures, such as SOEC[8,14,69] or oxygen transport membranes,[62] by using the heated plasma exhaust to activate a downstream product separation.

Numerical modeling

We applied our chemical kinetics model to our experimental conditions presented in previous section, and Figure 2A presents the calculated CO and O_2 concentrations as a function of position in (and after) the plasma region. The measured concentrations (downstream, hence after the plasma) are indicated with stars for comparison. An O_2 concentration of 6.2% is predicted at ~35 cm, 15 cm outside the plasma region, which extends from 0 to 20 cm. This compares reasonably well to the value of 5.2% ± 0.5% measured in our experiment (see star in Figure 2). The CO concentration predicted by our model is approximately twice the O_2 concentration at a value of 12.5% at ~35 cm, as shown in Figure 2. This value also compares reasonably to our experimental measurement of 9.7% ± 0.9%.

Because of this reasonable agreement between model and experiments, we can use the model to analyze the dominant CO and O_2 production reactions. Averaged across the simulation domain, both CO and O_2 are primarily formed via Equation 13, involving the collision of O atoms with CO_2 and yielding CO and O_2. Our analysis

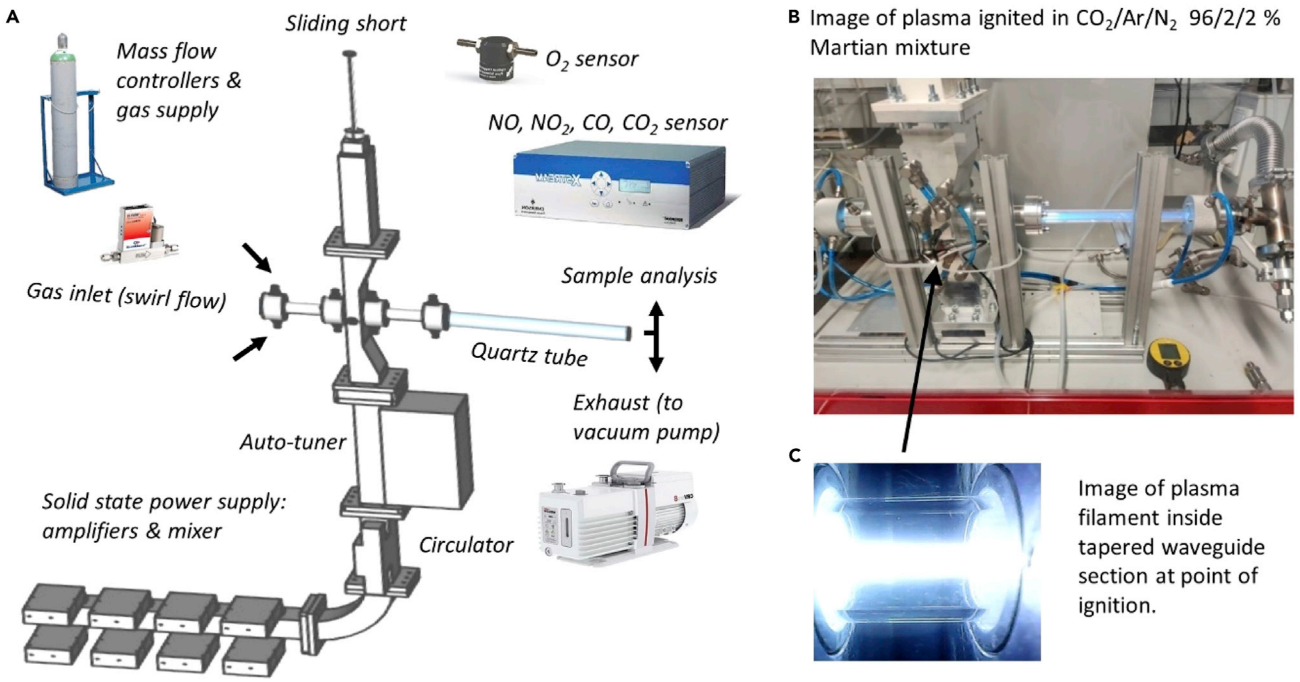

Figure 3. Experiment setup

(A) Illustration of our MW reactor consisting of a solid-state MW power supply, circulator, auto-tuner, and tapered waveguide section terminated by a sliding short. The plasma is ignited inside a quartz tube, where a swirling flow is injected. Sample analysis of the exhaust gas was carried out with non-dispersive infrared (NDIR) spectrometry and a luminescence O_2 sensor.

(B) Photo of the reactor in operation with a Martian simulant atmosphere at 0.34 bar pressure and 1 kW power. Ignition takes place in a tapered section of a 2.45 GHz WR340 waveguide, where a plasma is suspended at the center of the tube.

(C) In-waveguide photo of the plasma; the camera viewpoint is looking toward the quartz tube inside the waveguide, as indicated by the arrow.

reveals that 85% of the CO and O_2 produced via Equation 13 involves the symmetric stretch and bending vibrational modes of CO_2, namely $CO_2(V_a–V_d)$ (0.08–0.33 eV in energy),[70] while 8% occurs from ground-state CO_2 and 7% originates from $CO_2(V_{1–21})$. This behavior is generally in agreement with previous reports on CO_2 conversion under similar (warm plasma) conditions.[58,71–73] Note that our model of course depends on input data, such as chemical reactions and corresponding rate coefficients and cross sections, but because this dominant CO_2-conversion mechanism is in agreement with the literature, we believe that our assumed chemistry is reliable. Other model assumptions and input data in the model, such as mass flow rate, pressure, reactor dimensions, and power density, match our experiments as closely as possible. For instance, the power density is determined by the plasma power divided by the plasma volume, both obtained from the experiment, and radial variations are incorporated to represent gas intersecting different regions of the plasma filament, as in our previous work.[36] The asymmetric stretch mode gives rise to the most efficient CO_2 dissociation pathway through a ladder-climbing mechanism. However, we see that this mode is relatively suppressed here (i.e., ~7% contribution) as a result of the relatively high pressures and temperatures under study (0.34 bar and 2,000–3,000 K in the plasma filament), which serve to strongly depopulate $CO_2(V)$ via vibrational-translational (VT) relaxation. Lower-pressure conditions would allow a much larger contribution of the asymmetric stretch mode, which as a result of its vibrationally higher energy can significantly reduce the energy cost of dissociation and thus provide improved efficiency. Pressure and temperature conditions more resemblant to the Martian ambient (i.e., ~0.01 bar, −60°C) should therefore serve to further increase the promising metrics discovered here. Because

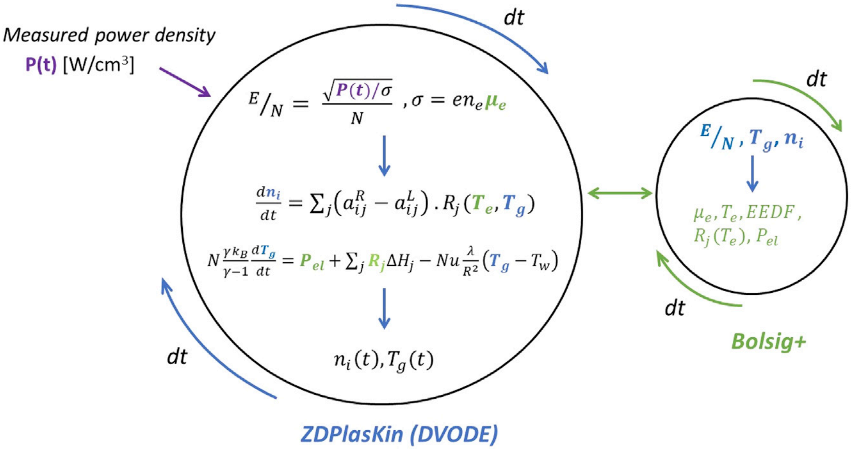

Figure 4. Overview of modeling scheme

Overview of the numerical solution scheme for the quasi-1D model employing ZDPlasKin, which incorporates the DVODE code for ordinary differential equation (ODE) integration and BOLSIG+ to solve the Boltzmann equation at each time step. An experimentally determined power density (W/cm^3) is coupled externally to enable solution via the reduced electric field E/N.

compressing the gas has an energy cost, it would be interesting to understand the influence of lower pressures on the results. Typically, plasma-based CO_2 conversion and NF are more energy efficient at lower pressures because of more pronounced vibrational-translational non-equilibrium, i.e., the vibrational levels of CO_2 and N_2, which give rise to the most efficient conversion,[20,21] are more overpopulated at lower pressure because of reduced losses upon collisions with the ground-state molecules. Our preliminary calculation results indeed confirm this better performance at lower pressure, but these results cannot yet be compared with experiments and are thus somewhat speculative. In our future work, we will investigate the effect of Martian pressures on the performance of both CO_2 conversion and NF.

Figure 2B shows that our model predicts a steady-state total NO_x concentration of ~311 ppm outside the plasma region at x ~ 35 cm. Comparatively, the total NO_x concentration in our experiment is measured as ~1,320 ppm; hence, our model clearly underestimates the NO_x production. Ramakers et al.[74] studied a CO_2/N_2 gliding arc plasma under similar conditions, and for the lowest N_2 fraction investigated (5%), they reported a NO_x concentration of about 1,500 ppm—very similar to our results. In addition, they also showed some discrepancy in absolute values between the simulated and measured NO_x concentration, but the trend as a function of N_2 fraction was correctly captured by the model. We believe that the discrepancy in absolute values is attributed to the low N_2 levels simulated, the complexity of the underlying chemistry (which relies on thousands of empirical reaction-rate data), and the inherent physical assumptions required in quasi-1D models of this kind. In spite of this, we believe that we can use the model to gain valuable insight into the underlying mechanisms.

We analyzed the dominant NO production reactions given NO's importance as the key NO_x species (i.e., measured NO/NO_2 ratio of ~3.4, and NO is a precursor for NO_2; see Equation 11). The Zeldovich reaction between N_2 and O atoms (Equation 9) is found to contribute 51% to the overall NO formation. This involves a contribution of 42.5% from electronically excited $N_2(E)$ (mainly $N_2(A^3\Sigma)$ at 6.2 eV and $N_2(B^3\prod)$ at 7.4 eV) and a contribution of 8.5% from the vibrationally excited $N_2(v)$ (mainly from the levels v = 10–14, which are near the threshold energy for N_2 oxidation). The other

Table 1. Species included in our quasi-1D model for a $CO_2/N_2/Ar$ mixture

Neutral	Excited	Charged
CO_2, CO, C_2O, C, C_2, CN, $ONCN$, NCO, NCN, C_2N, C_2N_2	$CO_2(V_a,V_b,V_c,V_d)$, $CO_2(V_1–V_{21})$, $CO_2(E_1)$, $CO(V_1–V_{10})$, $CO(E_1–E_4)$	CO_2^+, CO_4^+, CO^+, $C_2O_2^+$, $C_2O_3^+$, $C_2O_4^+$, C_2^+, C^+, CO_3^-, CO_4^-
O_2, O, O_3	$O_2(V_1–V_{15})$, $O_2(A_1\Delta)$, $O_2(A_3C_3C_1)$,[a] $O_2(B_1\Sigma)$, O(1D), O(1S)	e, O^+, O^-, O_2^-, O_2^+, O_4^-, O_4^+, O_3^-
N_2, N, NO_2, NO, N_2O, N_2O_3, N_2O_4, N_2O_5	$N_2(V_1–V_{21})$, $N_2(^2D)$, $N_2(^3P)$, $N_2(A_1\Sigma)$, $N_2(A_3\Sigma)$, $N_2(B_3\Pi)$, $N_2(C_3\Pi)$	N_2^+, N_3^+, N_4^+, N^+, NO_2^+, NO_2^-, N_2O^-, N_2O^+, NO^+, NO^-, NO_3^-
Ar	$Ar(^4S)$, $Ar(^4P)$, $Ar_2(E)$,[b] $Ar(^4S^3[P_0])$, $Ar(^4S^3[P_1])$, $Ar(^4S^3[P_2])$, $Ar(^4S^1[P_1])$	Ar^+, Ar_2^+

For details about the notations of the other excited levels, see our earlier work.[71,74,103]

[a] $O_2(A_3C_3C_1)$ is a combination of three electronically excited states $O_2(A^3\Sigma)$, $O_2(C^3\Delta)$, and $O_2(c^1\ \Sigma)$ with a threshold energy of 4.5 eV.

[b] $Ar_2(E)$ is a combination of the excited states $Ar_2(^1\Sigma)$ and $Ar_2(^3\Sigma)$ of the Ar_2 dimer.

Zeldovich reaction (Equation 10) is found on average to contribute ~18% to NO formation. The remainder NO is derived from non-Zeldovich reactions, including the reaction of N and its electronically excited state $N(^2D)$ with $CO_2/CO_2(V_{a–d})$ (contributing ~ 20%), while three-body reactions of N and O atoms with $CO_2/CO_2(V_{a–d})$ account for ~11%. In summary, the majority of NO formation is found to occur by a combination of the electronically and vibrationally enhanced Zeldovich reactions (Equations 9 and 10) with a total contribution of nearly 70%. This is beneficial because the electronically and vibrationally excited levels lower the energy thresholds of these reactions, thus contributing to energy-efficient NO_x formation. The Zeldovich reaction scheme for NO_x production, as predicted here, is a well-known reaction pathway for nitrogen oxidation. Indeed, this mechanism is consistent with our earlier works in both O_2/N_2 mixtures[36,75–78] and CO_2/N_2 mixtures,[74] giving us confidence in the model's capability to describe the chemical mechanisms despite the low NO_x levels predicted.

Finally, our model also provides information on other key plasma parameters, such as electron density and electron temperature: averaged over the plasma region (i.e., 0–20 cm), they were found to be $3.3 \times 10^{12}\ cm^{-3}$ and 0.51 eV, respectively. This is consistent with previous experimental reports on MW plasmas under similar conditions.[35,79]

Utilization scenarios

Future progress of plasma-based ISRU on Mars will need to not only capitalize on the promising metrics demonstrated here but also solve outstanding hurdles by integrating any plasma conversion process with efficient gas-separation technologies for a particular utilization scenario.[2] Adsorption techniques (i.e., pressure swing adsorption [PSA] or temperature swing adsorption [TSA]) for both CO and O_2 separation from $O_2/CO/CO_2$ and CO/CO_2 mixtures are an important separation technology in a Martian ISRU context.[80] Carbajo et al.[81] recently investigated the use of zeolite materials for separation of a typical plasma-produced $CO/O_2/CO_2$ mixture by using PSA. The authors showed that existing commercial materials should perform well (i.e., give reasonably high purity ~ 96%) under mild conditions (i.e., ~2 bar). The current energy cost of compression for MOXIE is about ~1–2 Wh/g CO_2[14,69,82] (pressure range = 0.34–1 bar), so a downstream PSA system to separate CO or O_2 is likely to have an energy cost on this order (i.e., ~1–2 Wh/g CO, O_2). In our case, the gas inlet flow rate is ~1,100 g/h CO_2, so the energy costs for compression for a downstream PSA stage are likely to be similar to the plasma conversion costs (i.e., per g O_2 or CO produced), yielding a total energy cost, including separation, in the order of ~0.04 kWh/g for O_2 production, or ~0.026 kWh/g for CO production, according to the promising metrics reported here. Hence, these combined costs could still fall significantly below MOXIE. However, this combination of plasma-based CO_2 splitting and PSA still needs to be tested in practice to confirm these numbers, which are now only theoretical estimates. Furthermore, these separation methods do not account for the NF part. A notable downside of adsorption techniques such as PSA is the difficulty of attaining very high purity (i.e., >96% O_2), which could be of concern for O_2 utilization in life support. Several consecutive adsorption and regeneration cycles would be necessary to increase purity,[83] leading to higher energy costs. However, given the estimates here, this could still be quite competitive with MOXIE. Further, the ambient low-pressure conditions on Mars could provide a "free" pressure differential (i.e., the technique known as vacuum pressure swing adsorption [VPSA]) to further reduce this energy overhead. Indeed, a MW plasma can be sustained across a wide pressure range (i.e., from ambient Martian pressures to above Earth ambient pressures) and deposits excess energy (not used in chemistry) as heat, providing a thermal energy source. This operational flexibility could be valuable for incorporation into any multi-stage adsorption configuration, where combinations of TSA, PSA, and VPSA could provide a rapid separation process (e.g., ~10–100 s)[84] amenable to coupling with intermittent (solar) electricity.

Combinations of plasma and SOEC, i.e., the technology of MOXIE, which decomposes and electrolyzes CO_2 and separates out the O_2 product,[14,69,82] could also offer an intriguing prospect for the production of highly purified O_2. Pandiyan et al.[85] recently interrogated the electrolysis of a CO_2 MW-plasma-exhaust mixture consisting of CO, O_2, and CO_2. The authors showed that O_2 separation, in particular, can be achieved exclusively at low overpotentials (i.e., <0.75 V) and reduced temperatures (i.e., ~650°C)—conditions where CO oxidation and CO_2 electrolysis (i.e., dissociation of CO_2) are not active. Using this combined plasma-SOEC approach, the authors reported a promising energy reduction of >50% for O_2 production (i.e., separation) compared with a pure CO_2 SOEC O_2 production. Feeding the SOEC cell with a $CO/O_2/CO_2$ (plasma) mix rather than pure CO_2 is also found to benefit the cells' durability considerably, with similarities to the methodology of partial recycling of exhaust CO used in MOXIE.[14] Notably, any plasma-SOEC hybrid technology operating at reduced temperatures (i.e., <650°C) would be much more flexible to powering by intermittent electricity sources and better exploit the operational flexibility of plasma conversion. MOXIE is currently limited in the number of thermal cycles, possibly as a result of material degradation,[14,69] so it cannot be easily switched on and off. Ongoing research efforts into low-temperature SOEC materials[86] could also have a significant impact on any future hybrid designs reaching more flexible operating conditions.

Obtaining a usable form of fixed nitrogen for farming on Mars could largely depend on the availability of water (e.g., extracted from Martian clays or regolith[87]). Water reacts readily with NO_2, a process exploited in the original B-E process, where NO is first oxidized to NO_2 in a settling tank before being hydrolyzed in a washing column to form a nitric acid solution. This could potentially solve the separation problem of the formed NO_x from the other gas components (CO, O_2, and unconverted CO_2 and N_2). Contemporary advances suggest that the energy cost and size of any adsorption stage could be significantly reduced, e.g., with modern NO_x absorbents such as BaO[88,89] in combination with PSA or TSA.[47] Nitric acid could be deployed directly for use in a hydroponic "soil-less" farm by serving as a direct source of nitrates for plant growth.[90] Applying an acid solution directly to soils in an open environment could lead to relatively poor uptake by plants as a result of the liquid's volatility. Soil-based Martian farms, as on Earth, are therefore likely to benefit from solid forms of nitrogen fertilizer. Combinations with urine are one possible pathway to form solid nitrogen fertilizer. Mixing nitric acid with urine reacts readily (i.e., exothermically) to form urea nitrate, a solid crystalline material that can be mixed into soils as a fertilizer. Further, the fermentation of urine can produce ammonia gas with the aid of the urease enzyme. Bubbling ammonia through nitric acid will readily (i.e., exothermically) produce the solid ammonium nitrate. Indeed, ammonium nitrate is the most common form of nitrogen fertilizer used today on Earth for soil-based farming. Notably, both urea nitrate and ammonium nitrate are also powerful explosives with potential utility for excavation activities by future settlers.

In summary, we emphasize that the promise of producing O_2 and CO while fixing nitrogen on Mars with the use of plasma technology combined with SOEC and/or adsorption methods is, at present, largely conceptual; however, we believe that this approach holds much potential for Mars ISRU, and we hope that this paper can inspire future research efforts.

Conclusions

We demonstrate the novel possibility of fixing N_2 on Mars, besides converting CO_2 to CO and O_2, by using the local Martian atmosphere. MW plasma conversion of the majority CO_2 fraction (∼96%) in the Martian atmosphere results in O atom formation, which enables oxidation of the small N_2 fraction (∼2%) and thus results in fixation of ∼7% of the N_2 present in a simulant Martian atmosphere. Our MW plasma investigation shows promising O_2, CO, and NO_x production rates of 47.0, 76.1, and 1.25 g/h, respectively, at an energy cost of 0.021, 0.013, and 0.79 kWh/g, respectively. Using the current energy allocation of 1 kWh available to MOXIE on NASA's Perseverance rover, our MW plasma produces 47.0 g/h of O_2, which is almost 30 times higher than the current capabilities of MOXIE (1.6 g/h) at a 10 times lower energy cost (0.021 versus 0.19 kWh/g). Plasma-based conversion therefore shows great potential as a future Martian ISRU technology.

This technology also has the key benefit of a rapid start-up time and is therefore highly flexible to the intermittent availability of Martian solar electricity (i.e., energy storage could be forgone). However, the energy costs reported only consider the plasma process and do not yet account for the cost of gas compression and separation, for which the combination with SOEC would be very interesting, especially because the hot plasma exhaust gas could activate a SOEC for downstream product separation. We hope this paper can inspire future research in this direction. Indeed, an efficient gas-separation technology downstream, in combination with our plasma technology, could generate the pure chemical streams for utilization as fertilizer, life support, and fuel for future robotic and human exploration of the red planet.

EXPERIMENTAL PROCEDURES

Resource availability

Lead contact

Further information and requests for resources and materials should be directed to and will be fulfilled by the lead contact, Seán Kelly (sean.kelly@uantwerpen.be).

Materials availability

This study did not generate new unique materials.

Data and code availability

Data from this study are available from the lead contact upon reasonable request.

Experimental setup

A schematic of our setup and an image of our MW plasma reactor in operation with a Martian simulant mixture consisting of 96% CO_2, 2% N_2, and 2% Ar are shown in Figures 3A and 3B. The power supply is composed of a collection of laterally diffused metal oxide semiconductor (LDMOS) power amplifiers, from which the output powers are combined in a mixer waveguide (WR340). This waveguide is connected via an isolator and an auto-tuner to a tapered waveguide section, including a 16 mm inner diameter quartz tube. The latter is mounted perpendicularly through a coupling hole (i.e., <1/4 wavelength in diameter), where the plasma ignition takes place. An auto-tuner, impedance analyzer, and adjustable short are used to tune the electric field to optimal conditions for electrical breakdown and to sustain a continuously powered plasma with minimum reflected power ($\ll$5%). Tangential gas injection ports coupled with a helical insert allow a swirl or vortex flow within the quartz discharge tube. Upon ignition, a surface wave sustained mode[91] is generated, with the plasma filament located at the tube center (see Figures 3B and 3C). This provides a key benefit by isolating the warm plasma ($\sim$2,000–3,000 K) from the quartz tube walls, allowing for elongated and stable plasma column formation along the tube lateral axis. Once initiated, the surface wave mode is stable across a wide pressure range from low pressures ($\sim$0.1 bar) to several bar.

Analysis of the NO_x species (i.e., NO and NO_2) and CO in the exhaust gas was performed with non-dispersive infrared and ultra-violet (NDIR/UV) absorption spectrometry (Rosemount X-STREAM XEGP Continuous Gas Analyzer[92]), while O_2 was measured with a PyroScience GmbH[93] sensor according to an infrared luminescent quenched absorption technique. All diagnostics were calibrated with pre-mixed calibration gases (Air Liquide) and cross-checked with gas chromatography (GC) using the compact-GC instrument from Interscience. This GC has two channels, each with a thermal conductivity detector (TCD) using carboxen and molsieve columns (1,010 PLOT and 5A, respectively) for O_2, N_2, and CO detection, and two RT Q-bond columns (3 and 10 m length, respectively) for CO_2 detection.[94]

The primary gas converted in our experiments is CO_2 (96% of the Martian atmosphere), with oxidation of the small N_2 content (2%). The argon fraction (2%) is not converted because of its inertness. The key overall reactions for consideration are as follows:

$$CO_2 \rightarrow CO + 1/2\ O_2 \qquad \text{(Equation 1)}$$

$$O_2 + N_2 \rightarrow 2\ NO \qquad \text{(Equation 2)}$$

$$2\ O_2 + N_2 \rightarrow 2\ NO_2 \qquad \text{(Equation 3)}$$

In any gas conversion process, there is typically gas expansion or contraction as a result of the changes in stoichiometry. In our experiments, this results in an increase in the mass outflow. Indeed, given that CO_2 is the primary component of the gas fraction, plasma conversion to CO and O_2 results in an expansion of the inlet flow, which depends on the degree of conversion. Notably, the formation of NO_2 results in gas contraction; however, because of the relatively small fraction of N_2 and even smaller fraction of NO_2 formed than CO and O_2, this has a negligible effect in comparison with expansion from CO_2 conversion. Strategies for measuring the gas mass outflow can include direct measurement or inference of the degree of expansion or contraction with the use of dilution gases. In our case, given the dominance of CO_2 conversion, the degree of expansion can be inferred with the CO_2 conversion:

$$\alpha = 1 + 0.5 * \eta_{CO_2}^{converted} \qquad \text{(Equation 4)}$$

$$\eta_{CO_2}^{converted} = \frac{\eta_{CO_2}^{OFF} - \alpha * \eta_{CO_2}^{ON}}{\eta_{CO_2}^{OFF}}, \qquad \text{(Equation 5)}$$

where α represents the gas expansion factor (i.e., $\alpha > 1$), $\eta_{CO_2}^{converted}$ is the fraction of CO_2 converted, $\eta_{CO_2}^{OFF}$ is the fraction of CO_2 in the mixture when the plasma is off (i.e., 0.96 in our case), and $\eta_{CO_2}^{ON}$ is the measured CO_2 fraction when the plasma is on. Rearranging Equations 4 and 5, we can solve them to find α based on the measured CO_2:

$$\alpha = \frac{1.5 * \eta_{CO_2}^{OFF}}{\eta_{CO_2}^{OFF} + 0.5 * \eta_{CO_2}^{ON}} \qquad \text{(Equation 6)}$$

Subsequently, when knowing α, we obtain the CO_2 conversion by using Equation 5. The CO, O_2, and NO_x production rates are calculated on the basis of the percentage yield of each species measured in the exhaust and the corresponding mass flow rate adjusted for the gas expansion. The individual production rates are then calculated for CO, O_2, and NO_x (NO + NO_2) as follows:

$$PR_{CO,\,O_2,\,NO_x}(g/h) = \frac{\eta_{CO,\,O_2,\,NO_x} * \mu_{CO,\,O_2,\,NO_x}(g/mol) * \alpha * f_{in}\,(L/min)}{22.4(L/mol)} * 60(min/h), \qquad \text{(Equation 7)}$$

where the production rate (PR [g/h]) is determined by the inlet mass flow rate (f_{in} [L/min]) for the Martian atmosphere simulant mix, consisting of 96% CO_2, 2% N_2, and 2% Ar. $\eta_{CO,\,O_2,\,NO_x}$ represents the fraction of species produced, directly measured in the plasma exhaust; $\mu_{CO,\,O_2,\,NO_x}$ (g/mol) is the molar mass of CO, O_2, or NO_x; and 22.4 (L/mol) is the molar volume of a gas under the corresponding standard conditions (i.e., standard temperature and pressure) for which our mass flow controllers are calibrated.

The energy cost for the production of CO, O_2, or NO_x is then obtained as follows:

$$EC_{CO,O_2,NO_x}(kWh/g) = \frac{power\ (kW)}{PR_{CO,\,O_2,\,NO_x}(g/h)}, \qquad \text{(Equation 8)}$$

where the power (kW or kJ/s) is the absorbed MW power measured during steady-state plasma operation.

Numerical modeling and chemistry

A quasi-1D chemical kinetics model is employed with the ZDPlasKin (Zero-Dimensional Plasma Kinetics) solver.[95–97] An overview of the simulation scheme is given in Figure 4, and full details of the equations employed are found in our earlier work.[36] The time evolution of the species densities, including electrons and various charged and neutral species, is calculated by balance equations considering the production and loss terms by chemical reactions. Dynamic changes in the gas velocity due to temperature and stoichiometric changes in the gas mixture are updated on each time step.

The power density P (W/cm^3) is derived from our experimental measurements of the absorbed power (i.e., forward minus reflected power), and the plasma volume is determined via camera imaging inside the tapered section of the waveguide (see Figures 3B and 3C). A cylindrical shape is assumed for the plasma volume.[98] This is consistent with vortex-stabilized discharges, where the plasma is contained within the tube inner region, separated from the containment walls by a swirling or vortex flow boundary. The plasma elongates along the direction of the flow (i.e., along the axial extent of the reactor tube) to form a cylindrical shape in its steady state.[34,98,99] In order to account for the radial variation in power density from the center of the plasma filament to its edge, the light emission across the radial extent of the plasma filament at its ignition point inside the waveguide (as shown in Figure 3C) is used as a proxy for the plasma width. We therefore solve the quasi-1D model for two different radial sections: a corresponding high power density of the plasma core and a relatively low power density to represent the plasma edge, as explained in our earlier paper.[36] For each of the quasi-1D models, we assume a triangular distribution of power density in the lateral extent of the plasma (i.e., along the direction of gas flow), in line with earlier modeling of power dissipation in surface-wave-sustained MW plasmas.[58,100]

The reduced electric field, i.e., the ratio of electric field over gas number density, a key fundamental variable defining the plasma characteristics, is calculated from our measured specified power density (see Figure 4). A Boltzmann solver (i.e., BOLSIG+) is utilized to simulate electron dynamics by linking the plasma conductivity (a function of the reduced electric field) to the electron mobility. Further to this, the gas temperature is solved in the model at each time step on the basis of gas heating due to elastic collisions of electrons with the gas molecules, the enthalpy contributions from the chemical reactions between all plasma species, heat losses to the walls, and the dynamic heat capacity accounting for the gas mixture. We calculate the radially averaged gas temperature (which is assumed to have a parabolic profile) by considering the time-dependent gas thermal balance equation under isobaric conditions. Further details can be found in our earlier works.[36,71,101,102]

The Martian air chemistry (i.e., $CO_2/N_2/Ar$) employed here is assembled from our earlier works.[71,74,103] The model includes 149 species, i.e., the electrons, CO_2, Ar, N_2, O_2, CO, various N_xO_y molecules in the ground state, and various (vibrational and electronic) excited levels, various radicals, atoms, and ions (see Table 1). These species react with each other in 973 electron-impact reactions and 12,604 heavy-particle reactions (i.e., between molecules in the ground-state or excited level, radicals, atoms, or ions). For the heavy-particle reactions, the rate coefficients are adopted from our earlier works, whereas the rate coefficients for the electron-impact reactions are calculated with the Boltzmann solver BOLSIG+[97] built in ZDPlasKin.

Plasma-based conversion of relatively inert molecules, such as N_2 and CO_2, provides unique reaction pathways not available in purely thermal conversion. Especially in MW plasma, the electrons have the right energy (~1 eV) to cause excitation toward the lowest vibrational levels in $CO_2/N_2/O_2$, followed by further vibrational-vibrational (V-V) collisions, which enable a "ladder-climbing" process, gradually populating higher vibrational levels (denoted as e.g., $CO_2(V)$ and $N_2(V)$). Further significant populations of electronically excited species (e.g., $CO_2(E)$ and $N_2(E)$) can form inside the plasma region. Such species serve to lower the overall energy required for CO_2 dissociation (i.e., O_2 formation) and NO_x formation because their higher energy levels help to overcome the activation barriers.

The underlying elementary reactions for NO_x production (see overall Equations 2 and 3 above) in a plasma involve the atoms formed upon dissociation of the corresponding molecules and proceed via the (electronically or vibrationally enhanced) Zeldovich mechanism,[53,104,105] consisting of the following reactions:

$$O + N_2/N_2(E,V) \leftrightarrow N + NO \qquad \text{(Equation 9)}$$

$$N + O_2/O_2(E,V) \leftrightarrow O + NO \qquad \text{(Equation 10)}$$

The above reaction pair is typically rate limited by Equation 9 given the energy requirement for overcoming the strong N_2 triple bond. Notably, the mechanism here can be significantly different from the purely thermal Zeldovich mechanism (i.e., involving only ground-state N_2 and O_2) as a result of the presence of vibrationally or electronically excited N_2 and O_2 molecules, available in plasmas. The vibrationally or electronically excited N_2 molecules lower the dissociation threshold required for breaking the N_2 bond (~9.8 eV) through colliding with O atoms (i.e., Equation 9). The N atoms formed in Equation 9 can then further react with both ground-state and vibrationally or electronically excited O_2 molecules (Equation 10) to produce another NO. Equation 10 also produces an additional O atom, which can again react with ground-state and vibrationally or electronically excited N_2 molecules (i.e., Equation 9) or oxidize NO to produce NO_2 (Equation 11):

$$NO + O \rightarrow NO_2 \qquad \text{(Equation 11)}$$

A similar oxidation pathway applies to CO_2. The overall Equation 1 above includes the following elementary reactions, involving atomic oxygen:

$$CO_2(E,V) \rightarrow CO + O \qquad \text{(Equation 12)}$$

$$CO_2(E,V) + O \rightarrow CO + O_2 \qquad \text{(Equation 13)}$$

Direct dissociation processes in Equation 12, such as electron-impact dissociation, have an energy threshold of 5.5 eV to overcome the (ground-state) CO_2 bond energy, but the atomic oxygen produced in Equation 12 can further react (i.e., Equation 13) with CO_2 (and its vibrationally or electronically excited states). This coupling lowers the threshold considerably (e.g., for the ground-state CO_2, this lowers the overall energy threshold to 2.9 eV[35]).

SUPPLEMENTAL INFORMATION

Supplemental information can be found online at https://doi.org/10.1016/j.chempr.2022.07.015.

ACKNOWLEDGMENTS

We acknowledge financial support by a European Space Agency (ESA) Open Science Innovation Platform study (contract no. 4000137001/21/NL/GLC/ov), the European Marie Skłodowska-Curie Individual Fellowship “PENFIX” within Horizon 2020 (grant no. 838181), the European Research Council (ERC) under the European Union’s Horizon 2020 Research and Innovation Program (grant no. 810182; SCOPE ERC Synergy project), and the Excellence of Science FWO-FNRS project (FWO grant no. GoF9618n and EOS no. 30505023). C.V. was supported by a FWO aspirant PhD fellowship (grant no. 1184820N). The calculations were performed with the Turing HPC infrastructure at the CalcUA core facility of the Universiteit Antwerpen (Uantwerpen), a division of the Flemish Supercomputer Centre VSC, funded by the Hercules Foundation, the Flemish government (department EWI), and Uantwerpen. We thank Dr. Waldo Bongers and Dr. Floran Peeters of DIFFER for their help and advice in the initial phase of the project; Mr. Luc van ‘t dack, Dr. Karen Leyssens, and Ing. Karel Venken for their adept technical assistance; Arn Van

Hemelen for his work on the project during his bachelor studies; Dr. Kevin van 't Veer and Dr. Josh Boothroyd for their helpful discussions and assistance with the modeling; Dr. Klaus Werner of PinkRF for discussions on solid-state MW technology; Dr. Pluton Pullumbi and Dr. Pascal Barbier of Air Liquide for discussions on gas-separation technologies; and Dr. Brandon Buergler of the ESA for discussions regarding solid oxide electrolysis technology.

AUTHOR CONTRIBUTIONS

S.K. conducted the experiments and modeling, including data analysis; S.K., A.C., and A.B. wrote the paper; and C.V. conducted modeling and compiled the chemistry.

DECLARATION OF INTERESTS

The authors declare no competing interests.

Received: January 24, 2022
Revised: March 21, 2022
Accepted: July 14, 2022
Published: August 22, 2022

REFERENCES

1. Foing, B.H. (2018). Reaction: Surviving on the Moon, Mars, and asteroids. Chem *4*, 14–15. https://doi.org/10.1016/j.chempr.2017.12.020.
2. Sanders, G.B., Paz, A., Oryshchyn, L., Araghi, K., Muscatello, A., Linne, D.L., Kleinhenz, J.E., and Peters, T. Mars ISRU for production of mission critical consumables – Options, recent studies, and current state of the art. In AIAA SPACE 2015 Conference and Exposition. 10.2514/6.2015-4458.
3. Hepp, A.F., Palaszewski, B.A., Colozza, A.J., Landis, G.A., Jaworske, D.A., and Kulis, M.J. (2014). In-situ resource utilization for space exploration: Resource processing, mission-enabling technologies, and lessons for sustainability on Earth and beyond. In 12th International Energy Conversion Engineering Conference (American Institute of Aeronautics and Astronautics). https://doi.org/10.2514/6.2014-3761.
4. Schlüter, L., and Cowley, A. (2020). Review of techniques for in-situ oxygen extraction on the moon. Planet. Space Sci. *181*, 104753. https://doi.org/10.1016/j.pss.2019.104753.
5. Starr, S.O., and Muscatello, A.C. (2020). Mars in situ resource utilization: A review. Planet. Space Sci. *182*, 104824. https://doi.org/10.1016/j.pss.2019.104824.
6. Casini, A.E.M., Maggiore, P., Viola, N., Basso, V., Ferrino, M., Hoffman, J.A., and Cowley, A. (2018). Analysis of a Moon outpost for Mars enabling technologies through a virtual reality environment. Acta Astronaut. *143*, 353–361. https://doi.org/10.1016/j.actaastro.2017.11.023.
7. Drake, B.G., Hoffman, S.J., and Beaty, D.W. (2010). Human exploration of Mars, Design Reference Architecture 5.0, pp. 1–24. March 6–13, 2010.
8. Sridhar, K.R., and Vaniman, B.T. (1997). Oxygen production on Mars using solid oxide electrolysis. Solid State Ionics *93*, 321–328. https://doi.org/10.1016/S0167-2738(96)00513-9.
9. European Space Agency (2021). Ariane 5G payload average cost kg/$ for 24 missions (Aerospace Security). https://aerospace.csis.org/data/space-launch-to-low-earth-orbit-how-much-does-it-cost/.
10. Rapp, D. (2015). Human Missions to Mars: Enabling Technologies for Exploring the Red Planet (Springer). https://doi.org/10.1007/978-3-319-22249-3.
11. European Space Agency. Exomars programme. https://exploration.esa.int/s/wKQB3q8.
12. Schulze-Makuch, D., Heller, R., and Guinan, E. (2020). In search for a planet better than Earth: Top contenders for a superhabitable world. Astrobiology *20*, 1394–1404. https://doi.org/10.1089/ast.2019.2161.
13. National Aeronautical Space Agency (2020). Mars Oxygen *In Situ* Resource Utilization Experiment (MOXIE). https://mars.nasa.gov/mars2020/spacecraft/instruments/moxie/.
14. Hecht, M., Hoffman, J., Rapp, D., McClean, J., SooHoo, J., Schaefer, R., Aboobaker, A., Mellstrom, J., Hartvigsen, J., Meyen, F., et al. (2021). Mars Oxygen ISRU Experiment (MOXIE). Space Sci. Rev. *217*, 9. https://doi.org/10.1007/s11214-020-00782-8.
15. Massachusetts Institute of Technology (2021). Aboard NASA's Perseverance rover, MOXIE creates oxygen on Mars. https://news.mit.edu/2021/aboard-nasa-perseverance-mars-rover-moxie-creates-oxygen-0421.
16. Loer, S.A., Scheeren, T.W.L., and Tarnow, J. (1997). How much oxygen does the human lung consume? Anesthesiology *86*, 532–537. https://doi.org/10.1097/00000542-199703000-00004.
17. Nelson, M., and Dempster, W.F. (1995). Living in space: Results from Biosphere 2's initial closure, an early testbed for closed ecological systems on Mars. Life Support Biosph. Sci. *2*, 81–102.
18. Linne, D. Carbon monoxide and oxygen combustion experiments—a demonstration of Mars in situ propellants. In 27th Joint Propulsion Conference. 10.2514/6.1991-2443.
19. Ash, R.L., Dowler, W.L., and Varsi, G. (1978). Feasibility of rocket propellant production on Mars. Acta Astronaut. *5*, 705–724. https://doi.org/10.1016/0094-5765(78)90049-8.
20. Bogaerts, A., and Neyts, E.C. (2018). Plasma technology: An emerging technology for energy storage. ACS Energy Lett. *3*, 1013–1027. https://doi.org/10.1021/acsenergylett.8b00184.
21. Snoeckx, R., and Bogaerts, A. (2017). Plasma technology—A novel solution for CO_2 conversion? Chem. Soc. Rev. *46*, 5805–5863. https://doi.org/10.1039/c6cs00066e.
22. Haberle, R.M. (2017). The Atmosphere and Climate of Mars (Cambridge University Press). https://doi.org/10.1017/9781139060172.
23. Franz, H.B., Trainer, M.G., Wong, M.H., Manning, H.L.K., Stern, J.C., Mahaffy, P.R., Atreya, S.K., Benna, M., Conrad, P.G., Harpold, D.N., et al. (2014). Analytical techniques for retrieval of atmospheric composition with the quadrupole mass spectrometer of the sample analysis at Mars instrument suite on Mars Science Laboratory. Planet. Space Sci. *96*, 99–113. https://doi.org/10.1016/j.pss.2014.03.005.
24. Wu, D., Outlaw, R.A., and Ash, R.L. (1996). Extraction of oxygen from CO_2 using glow-discharge and permeation techniques. J. Vac.

Sci. Technol. A *14*, 408–414. https://doi.org/10.1116/1.580098.

25. Gruenwald, J. (2014). Human outposts on Mars: Engineering and scientific lessons learned from history. CEAS Space J. *6*, 73–77. https://doi.org/10.1007/s12567-014-0059-8.

26. Gruenwald, J. (2016). A hybrid plasma technology life support system for the generation of oxygen on Mars: Considerations on materials and geometry. Acta Astronaut. *123*, 188–191. https://doi.org/10.1016/j.actaastro.2016.03.021.

27. Guerra, V., Silva, T., Ogloblina, P., Grofulović, M., Terraz, L., Silva, M.L.d., Pintassilgo, C.D., Alves, L.L., and Guaitella, O. (2017). The case for *in situ* resource utilisation for oxygen production on Mars by non-equilibrium plasmas. Plasma Sources Sci. Technol. *26*, 11LT01. https://doi.org/10.1088/1361-6595/aa8dcc.

28. Ogloblina, P., Morillo-Candas, A.S., Silva, A.F.S.d., Silva, T.P., Tejero-del-Caz, A., Alves, L.L., Guaitella, O., and Guerra, V. (2021). Mars *in situ* oxygen and propellant production by non-equilibrium plasmas. Plasma Sources Sci. Technol. *30*, 065005.

29. Premathilake, D., Outlaw, R.A., Quinlan, R.A., and Byvik, C.E. (2019). Oxygen generation by carbon dioxide glow discharge and separation by permeation through ultrathin silver membranes. Earth Space Sci. *6*, 557–564. https://doi.org/10.1029/2018EA000521.

30. Moses, R.W., Kuhl, C.A., and Templeton, J. (2005). Plasma assisted ISRU at Mars, held in Moscow.

31. Wheeler, R.R.J., Hadley, N.M., Wambolt, S.R., Holtsnider, J.T., Dewberry, R., and Karr, L.J. (2015). Plasma extraction of oxygen from Martian atmosphere (PEOMA). https://ttu-ir.tdl.org/bitstream/handle/2346/64474/ICES_2015_submission_203.pdf?sequence=1.

32. Fridman, A. (2008). Plasma Chemistry (Cambridge University Press). https://doi.org/10.1017/cbo9780511546075.

33. Bogaerts, A., and Centi, G. (2020). Plasma technology for CO_2 conversion: A personal perspective on prospects and gaps. Front. Energy Res. *8*, 111. https://doi.org/10.3389/fenrg.2020.00111.

34. Wolf, A.J., Righart, T.W.H., Peeters, F.J.J., Groen, P.W.C., van de Sanden, M.C.M., and Bongers, W.A. (2019). Characterization of CO_2 microwave plasma based on the phenomenon of skin-depth-limited contraction. Plasma Sources Sci. Technol. *28*, 115022. https://doi.org/10.1088/1361-6595/ab4e61.

35. Bongers, W., Bouwmeester, H., Wolf, B., Peeters, F., Welzel, S., van den Bekerom, D., den Harder, N., Goede, A., Graswinckel, M., Groen, P.W., et al. (2017). Plasma-driven dissociation of CO_2 for fuel synthesis. Plasma Processes Polym. *14*, 1600126. https://doi.org/10.1002/ppap.201600126.

36. Kelly, S., and Bogaerts, A. (2021). Nitrogen fixation in an electrode-free microwave plasma. Joule *5*, 3006–3030. https://doi.org/10.1016/j.joule.2021.09.009.

37. Winter, L.R., and Chen, J.G. (2021). N_2 fixation by plasma-activated processes. Joule *5*, 300–315. https://doi.org/10.1016/j.joule.2020.11.009.

38. Wamelink, G.W.W., Frissel, J.Y., Krijnen, W.H.J., Verwoert, M.R., and Goedhart, P.W. (2014). Can plants grow on Mars and the moon: A growth experiment on Mars and moon soil simulants. PLoS ONE *9*, e103138. https://doi.org/10.1371/journal.pone.0103138.

39. Eichler, A., Hadland, N., Pickett, D., Masaitis, D., Handy, D., Perez, A., Batcheldor, D., Wheeler, B., and Palmer, A. (2021). Challenging the agricultural viability of Martian regolith simulants. Icarus *354*, 114022. https://doi.org/10.1016/j.icarus.2020.114022.

40. Fackrell, L.E., Schroeder, P.A., Thompson, A., Stockstill-Cahill, K., and Hibbitts, C.A. (2021). Development of Martian regolith and bedrock simulants: Potential and limitations of Martian regolith as an *in-situ* resource. Icarus *354*, 114055. https://doi.org/10.1016/j.icarus.2020.114055.

41. Wamelink, G.W.W., Frissel, J.Y., Krijnen, W.H.J., and Verwoert, M.R. (2019). Crop growth and viability of seeds on Mars and Moon soil simulants. Open Agric. *4*, 509–516. https://doi.org/10.1515/opag-2019-0051.

42. Certini, G., Karunatillake, S., Zhao, Y.-Y.S., Meslin, P.-Y., Cousin, A., Hood, D.R., and Scalenghe, R. (2020). Disambiguating the soils of Mars. Planet. Space Sci. *186*, 104922. https://doi.org/10.1016/j.pss.2020.104922.

43. Mancinelli, R.L., and Banin, A. (2003). Where is the nitrogen on Mars? Int. J. Astrobiol. *2*, 217–225. https://doi.org/10.1017/S1473550403001599.

44. Silverstone, S.E. (1997). Food production and nutrition for the crew during the first 2-year closure of Biosphere 2. Life Support Biosph. Sci. *4*, 167–178.

45. Lim, S., Rood, C., and Hassanalian, M. (2020). Examination of explosives in Martian atmospheric conditions. In AIAA Propulsion and Energy 2020 Forum (American Institute of Aeronautics and Astronautics). https://doi.org/10.2514/6.2020-3652.

46. Dick, R.D., Fourney, W.L., Goodings, D.J., Lin, C.-P., and Bernold, L.E. (1992). Use of explosives on the moon. J. Aerosp. Eng. *5*, 59–69.

47. Rouwenhorst, K.H.R., Jardali, F., Bogaerts, A., and Lefferts, L. (2021). From the Birkeland-Eyde process towards energy-efficient plasma-based NOx synthesis: A techno-economic analysis. Energy Environ. Sci. *14*, 2520–2534. https://doi.org/10.1039/d0ee03763j.

48. Patil, B.S., Wang, Q., Hessel, V., and Lang, J. (2015). Plasma N_2-fixation: 1900–2014. Cat. Today *256*, 49–66. https://doi.org/10.1016/j.cattod.2015.05.005.

49. Chen, J.G., Crooks, R.M., Seefeldt, L.C., Bren, K.L., Bullock, R.M., Darensbourg, M.Y., Holland, P.L., Hoffman, B., Janik, M.J., Jones, A.K., et al. (2018). Beyond fossil fuel–driven nitrogen transformations. Science *360*, eaar6611. https://doi.org/10.1126/science.aar6611.

50. Birkeland, K. (1906). On the oxidation of atmospheric nitrogen in electric arcs. Trans. Faraday Soc. *2*, 98–116. https://doi.org/10.1039/TF9060200098.

51. Cherkasov, N., Ibhadon, A.O., and Fitzpatrick, P. (2015). A review of the existing and alternative methods for greener nitrogen fixation. Chem. Eng. Process.: Process Intensif. *90*, 24–33. https://doi.org/10.1016/j.cep.2015.02.004.

52. Eyde, H.S. (1909). The Manufacture of nitrates from atmosphere by the electric arc—Birkeland-Eyde process. J. R. Soc. Arts *57*, 568–576.

53. Wang, W., Patil, B., Heijkers, S., Hessel, V., and Bogaerts, A. (2017). Nitrogen fixation by gliding arc plasma: Better insight by chemical kinetics modelling. ChemSusChem *10*, 2145–2157. https://doi.org/10.1002/cssc.201700095.

54. Knox, J. (1914). The Fixation of Atmospheric Nitrogen (Gurney & Jackson).

55. Horikoshi, S., and Serpone, N. (2020). RF Power Semiconductor Generator Application in Heating and Energy Utilization (Springer).

56. Werner, K., and Theeuwen, S. (2012). RF driven plasma lighting: The next revolution in light sources. Microw. J. *53*, 68–74.

57. (HHF), H.H.-T.G. (2020). Jets PC-series plasma reactors. https://hhft.de/microwave-plasma.

58. Berthelot, A., and Bogaerts, A. (2017). Modeling of CO_2 splitting in a microwave plasma: How to improve the conversion and energy efficiency. J. Phys. Chem. C *121*, 8236–8251. https://doi.org/10.1021/acs.jpcc.6b12840.

59. Whittlesey, A.C., and Lumsden, J.M. (1981). Electric welding hazard to spacecraft electronics. In 1981 IEEE International Symposium on Electromagnetic Compatibility, pp. 1–5.

60. Bodeau, M. (2019). Mitigating potential hazards of TIG welding on spacecraft. IEEE Trans. Electromagn. Compat. *61*, 90–99.

61. Werner, K. (2020). Pink RF, RF energy solutions. https://www.pinkrf.com/products/power-amplifiers/.

62. Bai, W., Feng, J., Luo, C., Zhang, P., Wang, H., Yang, Y., Zhao, Y., and Fan, H. (2021). A comprehensive review on oxygen transport membranes: Development history, current status, and future directions. Int. J. Hydr. Energy *46*, 36257–36290. https://doi.org/10.1016/j.ijhydene.2021.08.177.

63. Liu, J., Ma, K., Ciais, P., and Polasky, S. (2016). Reducing human nitrogen use for food production. Sci. Rep. *6*, 30104. https://doi.org/10.1038/srep30104.

64. Zhang, X. (2017). A plan for efficient use of nitrogen fertilizers. Nature *543*, 322–323. https://doi.org/10.1038/543322a.

65. Rockström, J., Steffen, W., Noone, K., Persson, A., Chapin, F.S., Lambin, E.F., Lenton, T.M., Scheffer, M., Folke, C., Schellnhuber, H.J., et al. (2009). A safe operating space for humanity. Nature *461*, 472–475. https://doi.org/10.1038/461472a.

66. British Petroleum Company (2021). BP statistical review of world energy. https://www.bp.com/en/global/corporate/energy-economics/statistical-review-of-world-energy.html.

67. Ramírez, C.A., and Worrell, E. (2006). Feeding fossil fuels to the soil: An analysis of energy embedded and technological learning in the fertilizer industry. Resour. Conserv. Recy. *46*, 75–93. https://doi.org/10.1016/j.resconrec.2005.06.004.

68. Jouhara, H., Khordehgah, N., Almahmoud, S., Delpech, B., Chauhan, A., and Tassou, S.A. (2018). Waste heat recovery technologies and applications. Therm. Sci. Eng. Prog. *6*, 268–289. https://doi.org/10.1016/j.tsep.2018.04.017.

69. Meyen, F.E., Hecht, M.H., and Hoffman, J.A. (2016). Thermodynamic model of Mars Oxygen ISRU Experiment (MOXIE). Acta Astronaut. *129*, 82–87. https://doi.org/10.1016/j.actaastro.2016.06.005.

70. Kozák, T., and Bogaerts, A. (2014). Evaluation of the energy efficiency of CO_2 conversion in microwave discharges using a reaction kinetics model. Plasma Sources Sci. Technol. *24*, 015024. https://doi.org/10.1088/0963-0252/24/1/015024.

71. Heijkers, S., Snoeckx, R., Kozák, T., Silva, T., Godfroid, T., Britun, N., Snyders, R., and Bogaerts, A. (2015). CO_2 conversion in a microwave plasma reactor in the presence of N_2: Elucidating the role of vibrational levels. J. Phys. Chem. C *119*, 12815–12828. https://doi.org/10.1021/acs.jpcc.5b01466.

72. Vermeiren, V., and Bogaerts, A. (2019). Improving the energy efficiency of CO_2 conversion in nonequilibrium plasmas through pulsing. J. Phys. Chem. C *123*, 17650–17665. https://doi.org/10.1021/acs.jpcc.9b02362.

73. Vermeiren, V., and Bogaerts, A. (2020). Plasma-based CO_2 conversion: To quench or not to quench? J. Phys. Chem. C *124*, 18401–18415. https://doi.org/10.1021/acs.jpcc.0c04257.

74. Ramakers, M., Heijkers, S., Tytgat, T., Lenaerts, S., and Bogaerts, A. (2019). Combining CO_2 conversion and N_2 fixation in a gliding arc Plasmatron. J. CO_2 Util. *33*, 121–130. https://doi.org/10.1016/j.jcou.2019.05.015.

75. Jardali, F., Van Alphen, S., Creel, J., Ahmadi Eshtehardi, H., Axelsson, M., Ingels, R., Snyders, R., and Bogaerts, A. (2021). NOx production in a rotating gliding arc plasma: Potential avenue for sustainable nitrogen fixation. Green Chem. *23*, 1748–1757. https://doi.org/10.1039/d0gc03521a.

76. Van Alphen, S., Jardali, F., Creel, J., Trenchev, G., Snyders, R., and Bogaerts, A. (2021). Sustainable gas conversion by gliding arc plasmas: A new modelling approach for reactor design improvement. Sustainable Energy Fuels *5*, 1786–1800. https://doi.org/10.1039/D0SE01782E.

77. Vervloessem, E., Aghaei, M., Jardali, F., Hafezkhiabani, N., and Bogaerts, A. (2020). Plasma-based N_2 fixation into NOx: Insights from modeling toward optimum yields and energy costs in a gliding arc Plasmatron. ACS Sustainable Chem. Eng. *8*, 9711–9720. https://doi.org/10.1021/acssuschemeng.0c01815.

78. Van Alphen, S., Ahmadi Eshtehardi, H., O'Modhrain, C., Bogaerts, J., Van Poyer, H., Creel, J., Delplancke, M.-P., Snyders, R., and Bogaerts, A. (2022). Effusion nozzle for energy-efficient NOx production in a rotating gliding arc plasma reactor. Chem. Eng. J. *443*, 136529. https://doi.org/10.1016/j.cej.2022.136529.

79. van den Bekerom, D.C.M., Linares, J.M.P., Verreycken, T., van Veldhuizen, E.M., Nijdam, S., Berden, G., Bongers, W.A., van de Sanden, M.C.M., and van Rooij, G.J. (2019). The importance of thermal dissociation in CO_2 microwave discharges investigated by power pulsing and rotational Raman scattering. Plasma Sources Sci. Technol. *28*, 055015. https://doi.org/10.1088/1361-6595/aaf519.

80. Walton, K., and LeVan, M. (2004). Separation of carbon monoxide and carbon dioxide for Mars ISRU. https://ntrs.nasa.gov/api/citations/20010024956/downloads/20010024956.pdf.

81. Perez-Carbajo, J., Matito-Martos, I., Balestra, S.R.G., Tsampas, M.N., van de Sanden, M.C.M., Delgado, J.A., Águeda, V.I., Merkling, P.J., and Calero, S. (2018). Zeolites for CO_2–CO–O_2 separation to obtain CO_2-neutral fuels. ACS Appl. Mater. Interfaces *10*, 20512–20520. https://doi.org/10.1021/acsami.8b04507.

82. Hinterman, E., and Hoffman, J.A. (2020). Simulating oxygen production on Mars for the Mars oxygen *in-situ* resource utilization experiment. Acta Astronaut. *170*, 678–685. https://doi.org/10.1016/j.actaastro.2020.02.043.

83. Luna-Triguero, A., Vicent-Luna, J.M., Jansman, M.J., Zafeiropoulos, G., Tsampas, M.N., van de Sanden, M.C.M., Akse, H.N., and Calero, S. (2021). Enhancing separation efficiency in European syngas industry by using zeolites. Cat. Today *362*, 113–121. https://doi.org/10.1016/j.cattod.2020.03.061.

84. Hedin, N., Andersson, L., Bergström, L., and Yan, J. (2013). Adsorbents for the post-combustion capture of CO_2 using rapid temperature swing or vacuum swing adsorption. Appl. Energy *104*, 418–433. https://doi.org/10.1016/j.apenergy.2012.11.034.

85. Pandiyan, A., Kyriakou, V., Neagu, D., Welzel, S., Goede, A., van de Sanden, M.C.M., and Tsampas, M.N. (2022). CO_2 conversion via coupled plasma-electrolysis process. J. CO_2 Util. *57*, 101904. https://doi.org/10.1016/j.jcou.2022.101904.

86. Wachsman, E.D., and Lee, K.T. (2011). Lowering the temperature of solid oxide fuel cells. Science *334*, 935–939. https://doi.org/10.1126/science.1204090.

[87]. Abbud-Madrid, A., Beaty, D.W., Boucher, D., Bussey, B., Davis, R., Gertsch, L., et al. (2016). Report of the Mars Water In-Situ Resource Utilization (ISRU) Planning (M-WIP) Study (California Institute of Technology). https://www.nasa.gov/sites/default/files/atoms/files/mars_water_isru_planning.pdf.

88. Schmitz, P.J., and Baird, R.J. (2002). NO and NO_2 adsorption on barium oxide: Model study of the trapping stage of NOx conversion via lean NOx traps. J. Phys. Chem. B *106*, 4172–4180. https://doi.org/10.1021/jp0133992.

89. Fridell, E., Skoglundh, M., Westerberg, B., Johansson, S., and Smedler, G. (1999). NOxStorage in barium-containing catalysts. J. Cat. *183*, 196–209. https://doi.org/10.1006/jcat.1999.2415.

90. Cannon, K.M., and Britt, D.T. (2019). Feeding one million people on Mars. New Space *7*, 245–254. https://doi.org/10.1089/space.2019.0018.

91. Moisan, M., and Pelletier, J. (2006). Physics of Collisional Plasmas. Application to High Frequency Discharges [Physique des plasmas collisionnels. Application aux decharges haute frequence] (Springer). https://link.springer.com/content/pdf/bfm%3A978-94-007-4558-2%2F1.pdf.

92. Emerson Rosemount™ X-STREAM X2GP continuous gas analyzer. https://www.emerson.com/en-us/catalog/rosemount-x-stream-x2gp-continuous-gas-analyzer.

93. PyroScience GmbH (2021). Firesting O_2 sensor. https://www.pyroscience.com/en/.

94. Girard-Sahun, F., Biondo, O., Trenchev, G., van Rooij, G., and Bogaerts, A. (2022). Carbon bed post-plasma to enhance the CO_2 conversion and remove O_2 from the product stream. Chem. Eng. J. *442*, 136268. https://doi.org/10.1016/j.cej.2022.136268.

95. Pancheshnyi, S., Eismann, B., Hagelaar, G.J.M., and Pitchford, L.C. (2008). Computer Code ZDPlasKin (University of Toulouse). www.zdplaskin.laplace.univ-tlse.fr.

96. Thompson, G.D.B.a.S. (2013). DVODE solver—Ordinary differential equation (ode) solver—a Fortran 90 version of the well-known VODE ode solver by Brown, Byrne, and Hindmarsh. http://www.radford.edu/thompson/vodef90web.html.

97. Hagelaar, G.J.M., and Pitchford, L.C. (2005). Solving the Boltzmann equation to obtain electron transport coefficients and rate coefficients for fluid models. Plasma Sources Sci. Technol. *14*, 722–733. https://doi.org/10.1088/0963-0252/14/4/011.

98. Van Alphen, S., Vermeiren, V., Butterworth, T., van den Bekerom, D.C.M., van Rooij, G.J., and Bogaerts, A. (2020). Power pulsing to maximize vibrational excitation efficiency in N_2 microwave plasma: A combined experimental and computational study. J. Phys. Chem. C *124*, 1765–1779. https://doi.org/10.1021/acs.jpcc.9b06053.

99. Wolf, A.J., Righart, T.W.H., Peeters, F.J.J., Bongers, W.A., and van de Sanden, M.C.M. (2020). Implications of thermo-chemical instability on the contracted modes in CO_2 microwave plasmas. Plasma Sources Sci. Technol. *29*, 025005. https://doi.org/10.1088/1361-6595/ab5eca.

100. Schlüter, H., and Shivarova, A. (2007). Travelling-wave-sustained discharges. Phys. Rep. *443*, 121–255.

101. Kelly, S., van de Steeg, A., Hughes, A., van Rooij, G., and Bogaerts, A. (2021). Thermal instability and volume contraction in a pulsed microwave N_2 plasma at sub-atmospheric pressure. Plasma Sources Sci. Technol. *30*, 055005. https://doi.org/10.1088/1361-6595/abf1d6.

102. Snoeckx, R., Heijkers, S., Van Wesenbeeck, K., Lenaerts, S., and Bogaerts, A. (2016). CO_2 conversion in a dielectric barrier discharge plasma: N_2 in the mix as a helping hand or problematic impurity? Energy Environ. Sci. *9*, 999–1011. https://doi.org/10.1039/c5ee03304g.

103. Van Gaens, W.V., and Bogaerts, A. (2013). Kinetic modelling for an atmospheric pressure argon plasma jet in humid air. J. Phys. D: Appl. Phys. *46*, 275201. https://doi.org/10.1088/0022-3727/46/27/275201.

104. Patil, B.S., Rovira Palau, J., Hessel, V., Lang, J., and Wang, Q. (2016). Plasma nitrogen oxides synthesis in a milli-scale gliding arc reactor: Investigating the electrical and process parameters. Plasma Chem. Plasma Process. *36*, 241–257. https://doi.org/10.1007/s11090-015-9671-4.

105. Rashid Alievich, S. (2014). Selected works of Yakov Borisovich Zeldovich, volume I. In 26. Oxidation of Nitrogen in Combustion and Explosions, S.R. Alievich, ed. (Princeton University Press), pp. 404–410. https://doi.org/10.1515/9781400862979.404.